Photo-quantum Hall effect and light-induced charge transfer at the interface of graphene/InSe heterostructures

Mahabub A. Bhuiyan[1], Zakhar R. Kudrynskyi[1], Debarati Mazumder[1], Jake D.G. Greener[1], Oleg Makarovsky[1], Christopher J. Mellor[1], Evgeny E. Vdovin[1, 2], Benjamin A. Piot[3], Inna I. Lobanova[3], Zakhar D. Kovalyuk[4], Marina Nazarova[5, 6], Artem Mishchenko[5], Kostya S. Novoselov[5], Yang Cao[6-7], Laurence Eaves[1], Go Yusa[8], Amalia Patanè[1*]

[1] School of Physics and Astronomy, The University of Nottingham, Nottingham NG7 2RD, UK

[2] Institute of Microelectronics Technology and High Purity Materials, RAS, Chernogolovka 142432, Russia

[3] Laboratoire National des Champs Magnétiques Intenses, CNRS-UGA-UPS-INSA-EMFL, 25 rue des Martyrs, 38042 Grenoble, France

[4] Institute for Problems of Materials Science, The National Academy of Sciences of Ukraine, Chernivtsi Branch, Chernivtsi 58001, Ukraine

[5] School of Physics and Astronomy, University of Manchester, Oxford Road, Manchester M13 9PL, UK

[6] National Graphene Institute, University of Manchester, Oxford Road, Manchester M13 9PL, UK

[7] State Key Laboratory of Physical Chemistry of Solid Surface, College of Chemistry and Chemical Engineering, Collaborative Innovation Center of Chemistry for Energy Materials, Xiamen University, Xiamen, 361005, China

[8] Department of Physics, Tohoku University, Sendai 980-8578, Japan

*Corresponding authors:

amalia.patane@nottingham.ac.uk

The transfer of electronic charge across the interface of two van der Waals crystals can underpin the operation of a new class of functional devices. Amongst van der Waals semiconductors, an exciting and rapidly growing development involves the "post-transition" metal chalcogenide InSe. Here we report on field effect phototransistors where single layer graphene is capped with n-type InSe. These device structures combine the photosensitivity of InSe with the unique electrical properties of graphene. We show that the light-induced transfer of charge between InSe and graphene offers an effective method to increase or decrease the carrier density in graphene, causing a change in its resistance that is gate-controllable and only weakly dependent on temperature. We probe the charge transfer at the InSe/graphene interface by Hall effect and photoconductivity measurements, and demonstrate that light can induce a sign reversal of the quantum Hall voltage and photovoltaic effects in the graphene layer. These findings demonstrate the potential of light-induced charge transfer in gate-tunable InSe/graphene phototransistors for optoelectronics and quantum metrology.

1. Introduction

Atomically thin layers of van der Waals (vdW) crystals and their heterostructures offer unique opportunities to explore and manipulate the transfer of electronic charge at the interface of different materials and to create high-performance multi-functional devices for integration with photonic and electronic technologies.[1] VdW crystals have strong covalent bonding within the two-dimensional (2D) atomic planes and weak vdW attraction between the layers. These properties enable the fabrication of stable films down to monolayer thickness and the realization of a wide range of multi-layered structures, overcoming limitations of traditional semiconductor heterojunctions, such as incompatibility of the active layer and substrate due to lattice mismatch, defective interfaces, *etc*.[2] Ongoing research is exploring a wide range of 2D materials such as graphene, the wide-gap insulator hexagonal boron nitride (hBN),[1,2] the narrow band gap semiconductor black phosphorus (bP),[3,4] and transition metal dichalcogenides (TMDCs, *e.g.* MoS_2, WS_2, *etc*.).[5,6] Amongst these 2D materials, the "post-transition" metal monochalcogenides, such as InSe, are receiving increasing attention.[7-19] The γ-polytype phase of InSe has a band gap that increases markedly with decreasing layer thickness down to a single layer and an interband optical spectrum ranging from the violet to the infrared.[7-9] It has a Brillouin zone-centered conduction band with a relatively small in-plane electron effective mass ($m_c \sim 0.14 m_e$)[7] that has been exploited in high mobility ($\mu = 0.2$ m^2/Vs at 300K and 2 m^2/Vs at 2K) 2D field effect transistors (FETs)[9,10] and devices with quantum point contacts or electrostatically defined quantum dots.[11,18] In particular, InSe can act as an electrically and optically active layer to "modulation-dope"[13] and photosensitize[14] an adjacent graphene layer, and to induce a "giant" quantum Hall (QH) plateau in its magnetoresistance.[13] These phenomena

involve a transfer of electronic charge at the InSe/graphene interface and offer opportunities to explore a diverse range of new electrical and optical devices.

Here we report on the effects of light on the transport properties of field effect phototransistors in which a layer of graphene is partially capped with *n*-type InSe. We use a combination of optical and magneto-transport studies to demonstrate that the absorption of light by the InSe induces: i) either an increase or decrease of resistance in the graphene layer that is gate-tuneable, but only weakly affected by temperature in the range $T = 2K$ to 300K; ii) a reversal in the sign of the Hall voltage in the QH regime that can be controlled by an appropriate combination of gate voltages and optical illumination over a range of temperatures of up to ~ 200K; iii) photovoltaic effects due to a built-in electric field at the graphene/InSe interface. These effects arise from the sensitivity of the electrical conductivity of the graphene layer to electronic charges that are photo-generated in the InSe and transferred across the interface onto the graphene. This light-induced charge transfer offers an effective method to increase or decrease selectively the carrier density in the InSe-capped graphene. An optical induced transition from a hole- to an electron-carrier current is also achieved over an extended range of gate voltages, with potential for quantum metrology and high-photosensitive sensors and switches.

2. Results and discussion

2.1 Gate-tunable graphene transistors photosensitized with InSe

Figure 1a shows an optical image of one of our InSe/graphene heterostructure devices. The InSe layer forms a cap over one half of the graphene Hall bar. The two sections of the device comprising uncapped and InSe-capped graphene are in a "series" resistance configuration with the same electrical current, *I*, flowing through both of them (Figure 1b). Magneto-transport experiments were performed in two modes: (i) in darkness and (ii) with the device uniformly

illuminated by an unfocused He-Ne laser beam with a photon energy, $hv = 1.96$ eV, in excess of the band gap energy of bulk InSe, $E_g = 1.26$ eV at 300K (see Experimental Methods). The V_g-dependence of the low ($T = 2$ K) and room temperature ($T = 300$K) resistance, R_{xx}, of the uncapped and InSe-capped graphene was measured at zero applied magnetic field in darkness, see black curves in Figure 1c. For uncapped graphene, R_{xx} reaches a maximum at a positive gate voltage, $V_g = +21$ V at $T = 2$K, from which we deduce that the graphene is p-doped at $V_g = 0$V with $p = 1.6{\times}10^{12}$ cm^{-2} (Supplementary information S1). For InSe-capped graphene, the maximum of $R_{xx}(V_g)$ occurs at a lower gate voltage, $V_g = +7$V, shifted by $\Delta V_g \approx$ - 14 V relative to the peak for uncapped graphene, corresponding to a reduced hole density. The $R_{xx}(V_g)$ curve for the graphene-only section of the Hall bar does not change when its surface is illuminated with laser light. In contrast, for InSe-capped graphene, the maximum of $R_{xx}(V_g)$ shifts towards lower gate voltages at both $T = 2$K and 300K (red curves in Figure 1c). This shift, ΔV_g, is proportional to the light intensity at low levels, but saturates at $\Delta V_g \approx$ - 6 V for a light intensity $P > 10$ mW/mm^2. It corresponds to an increase in the electron density by $\Delta n = 4.5{\times}10^{11}$ cm^{-2} at $V_g = 0$ V (Supplementary Information S1).

The photosensivity of the InSe-capped graphene section of the device is illustrated in more detail in Figure 1d, which shows the V_g-dependence of the light-induced change of R_{xx}, i.e. $\Delta R_{xx} = R_{xx}$(light) - R_{xx}(dark), at $T = 2$K. ΔR_{xx} has a maximum at a gate voltage $V_L \sim$ 0V, passes through zero at a gate voltage $V_F \sim +6$ V and changes sign with a minimum at $V_D \sim +10$ V. The values of V_D and V_L correspond approximately to the peak positions of the $R_{xx}(V_g)$ curves in darkness and under illumination, respectively (Figure 1c). At the peak of $R_{xx}(V_g)$ the Fermi energy, E_F, aligns with the neutrality point of the graphene's band structure in darkness ($V_D \sim +10$ V) and under illumination ($V_L \sim 0$ V). The dependence of R_{xx} and ΔR_{xx} on V_g is weakly affected by

temperature, revealing similar features at both $T = 2$ and 300K (Figure 1c and Supplementary Information S1).

The data in Figure 1 show that in darkness the capping of graphene with InSe increases significantly the electron density in the graphene layer. Under illumination, the density of electrons in the InSe-capped graphene increases further. In particular, the similar form of the $R_{xx}(V_g)$ curves at low and room temperature indicates a relatively weak contribution of phonon scattering to the mobility of carriers. This behaviour can be accounted for by the dominant contribution of carrier scattering by negatively charged acceptor impurities in our CVD-graphene. [13] In the following sections, we use gate-dependent quantum Hall effect measurements to examine how the photogenerated electrons are distributed between the component layers of the InSe/graphene heterostructure.

2.2 Landau level quantization and photo-quantum Hall effect

The effects of light on the Hall resistance, R_{xy}, and its dependence on V_g are shown in Figure 2a for various magnetic fields, B, and $T = 2$K. For gate voltages in the range $V_L < V_g < V_D$ (see shaded areas), the optical excitation induces a sign reversal of the Hall voltage and of the QH plateau, $R_{xy} = h/ve^2$, where $v = 2$ is the graphene Landau level (LL) filling factor. Thus illumination induces a transition from a hole- to an electron-carrier current in the graphene layer over an extended range of gate voltages (Figure 2b).

We probe the distribution of charge in the graphene and InSe layers in the dark and under illumination by analyzing the magnetoresistance $R_{xx}(V_g)$ curves of the InSe-capped graphene layer, see Figure 3a-b. At low temperature ($T = 2$ K) and in the presence of a quantizing magnetic field, both in darkness (left panel, Figure 3a) and under illumination (right panel, Figure 3a), the

plots of $R_{xx}(V_g)$ display a pair of minima over a range of gate voltages corresponding to a quantized value of $R_{xy} = h/2\,e^2$. Furthermore, under illumination, the minima in R_{xx} and the corresponding width of the QH plateaux in R_{xy} become asymmetric, and the QH plateau at $V_g > 0$ V becomes almost twice as wide as in darkness (Figure 3b).

For single layer graphene, the energy-level spectrum of Dirac fermions in a magnetic field is described by the relation $E_i = sgn(i)\sqrt{ehv_F^2 B|i|/\pi}$, where $v_F \sim 10^6$ m/s is the Fermi velocity and $i = 0, \pm1, \pm2 \ldots$ The spectrum comprises electron ($i \geq 1$) and hole ($i \leq -1$) LLs, as well as a LL ($i = 0$) at the neutrality point (inset of Figure 3a).[20,21] Since the LLs for electrons and holes are symmetrically arranged around the $i = 0$ state, one might expect an approximately symmetric V_g-dependence of R_{xx} and R_{xy} relative to the voltage position of the peak in $R_{xx}(V_g)$. For graphene or InSe-capped graphene in darkness, the minima in R_{xx} and the corresponding width of the QH plateaux in R_{xy} at the LL filling factor $\nu = 2$ are indeed symmetric. However, for InSe-capped graphene under illumination, both peaks and plateaux become asymmetric (Figure 3b).

For the case of uncapped graphene and InSe-capped graphene in darkness, we use a simple capacitance equation, $i.e.$ $C = e[dn_G/dV_g]$, to calculate the voltage separation ΔV_g of the maxima in the $R_{xx}(V_g)$ curve at different B. Here $C = \varepsilon\varepsilon_0/t$ is the "classical" capacitance per unit area of the graphene/SiO$_2$/Si heterostructure, e is the elementary charge, $t = 285$ nm is the SiO$_2$ layer thickness, $\varepsilon = 3.9$ is the relative dielectric constant of SiO$_2$, ε_0 is the permittivity of free space, and n_G is the carrier density in the graphene layer. In our model, we have neglected the quantum capacitance, C_q, of graphene, which accounts for the non-classical dependence of n_G on the applied gate voltage when the Fermi energy, E_F, is close to the low density of states at the Dirac point: $C_q = 2e^2 E_F/\pi\hbar^2 v_F^2$. When the Fermi level is far from the Dirac point, the effect of the quantum capacitance becomes negligible (Supplementary information S4).

Over the range of V_g between the maxima M_0 and M_1 in $R_{xx}(V_g)$ (see Figure 3a), corresponding respectively to the alignment of the Fermi level with the $i = 0$ and $i = +1$ LLs, $\Delta V_g = eg/C$, where $g = 4eB/h$ is the LL degeneracy.[20] This simple model reproduces quite accurately the data for the uncapped graphene in darkness and under illumination at different values of B and also for InSe-capped graphene in darkness (Figure 3c, black dots and star). However, it does not reproduce the values of ΔV_g in InSe-capped graphene under illumination (Figure 3c, open circles). To explain this behavior, we note that when the positive gate voltage or the intensity of light are sufficiently large that the Fermi level approaches the InSe CB edge, electrons start to fill donor states below the CB edge. In this case the carrier density induced by V_g has two contributions, one from the InSe layer (n_{InSe}) and one from graphene (n_G). From the measured value of ΔV_g, corresponding to the separation of the peaks M_0 and M_1 peaks in R_{xx}, we estimate n_{InSe}, i.e. $en_{InSe} = C\Delta V_g - en_G$, where $n_G = 4eB/h$ and $C = \varepsilon\varepsilon_0/t$. The values of n_{InSe} are plotted in Figure 4d for different B: n_{InSe} increases with B from zero at $B = 0$T and $V_g \approx 0$ V to 6×10^{11}cm^{-2} at $B = 6$T and $V_g \approx 15$ V. These values are comparable to the electron density in the $i = +1$ LL of the graphene layer, $n_G = 4eB/h$, also shown in Figure 3d. The increase of n_{InSe} with B corresponds to an increase of the Fermi energy from the Dirac point at $i = 0$ at $E_0 = 0$ to the $i = +1$ LL at $E_1 = \sqrt{e\hbar v_F^2 B/\pi}$. Thus, at low temperatures, a significant fraction of electrons become bound on the relatively large density of donors ($\sim 10^{11}$ cm^{-2}) in the InSe capping layer. These donor states are likely to extend over a broad energy range: we estimate that $E_1 - E_0 \sim 60$ meV at $B = 10$ T. The binding energy of isolated donors in bulk InSe is $E_d \sim 30$ meV.[17] However, for thin InSe, E_d depends on the position of the donors relative to the surface; furthermore, closely spaced donors can have larger binding energies. At low temperatures ($T < 100$ K) the electrons in

InSe remain bound to donors so that the QH voltage of the graphene layer is not "short-circuited" by the parallel conduction in the InSe layer.

The larger negative charge in the InSe-capped graphene with increasing positive gate voltage and/or increasing light intensity causes an asymmetric distribution of LL-features and QH plateaus relative to the peak in $R_{xx}(V_g)$ (see Figure 3b). In particular, over a range of gate biases the QH plateau extends to high B. For example, at $V_g = 7.5$ V and $V_g = -6.0$ V, the QH plateau extends from $B \sim 5$T to 14 T at $T = 2$K, corresponding to an increase in sheet density of $\sim 5 \times 10^{11}$ cm^{-2} (Figure 4a), and persists over a wide range of temperatures (Figure 4b). We have observed this behavior for several devices although the QH resistance plateau occurs for gate voltages that vary slightly from sample to sample (Supplementary Information S2). The extended $v = 2$ QH plateau arises from the "pinning" of the chemical potential in the energy gap between Landau levels when their degeneracy increases with increasing B. This is facilitated by the close alignment of the conduction band edge of InSe with the Dirac point of graphene: The electron affinity of graphene ($\chi_{Gr} = 4.5$ eV) is only slightly smaller than that of bulk InSe ($\chi_{InSe} = 4.6$ eV)[13].

The extended QH plateau reported here is similar in form to that for graphene grown epitaxially by the thermal decomposition of the surface layer of SiC.[22-26] This phenomenon has be explained in terms of the transfer of charge carriers, between the graphene layer and defects in the adjacent SiC substrate.[26] The data reported here demonstrate that a similar process occurs between graphene and donors in the n-type InSe capping layer. Thus the $i = 0$ Landau level at the Dirac point of the graphene layer remains completely filled when its degeneracy increases with increasing B. Our data illustrate that this effect can be controlled by both the gate voltage and optical illumination. Although the $v = 2$ plateau in R_{xy} becomes weaker with increasing

temperature, it can be seen even up to temperatures of $T \sim 200K$ at $B = 14T$ (Figure 4b). We attribute the quenching of the QH plateau at higher T to the thermal ionization of electrons out of the donor states into the conduction band of the InSe capping layer, leading to thermally-activated parallel conduction in InSe (Supplementary Information S3).

2.3 Photocurrent maps of InSe-graphene heterostructures

To investigate in further detail the light-induced charge transfer at the InSe/graphene interface, we carried out a series of measurements to produce spatially resolved photocurrent maps of graphene-InSe-graphene planar devices. As shown in Figure 5a, in these devices the two graphene (G) layers serve as source (s) and drain (d) electrodes to an InSe channel of length $l \sim 1$ μm and width $w \sim 20$ μm. The InSe layer is encapsulated with a hBN layer, which also overlaps the two graphene layers. The room temperature photocurrent map is obtained by scanning a focused laser beam across the plane of the device with or without an applied source-drain bias voltage, V_{sd}. As shown in Figure 5b, for $V_{sd} = 0$, a photocurrent ΔI is generated in the InSe-capped graphene layers (see areas within the dashed lines in Figure 5b). This photocurrent is non-uniform, is enhanced at the graphene edges and has opposing polarities on the two graphene electrodes. These data indicate the presence of a built-in electric field at the graphene/InSe interface (bottom inset, Figure 5b) and that this field is stronger at the edges of the graphene electrodes. As shown in Figure 5c, the photocurrent increases for $V_{sd} > 0$: the photocurrent is generated in two distinct regions: the area of the InSe flake between the two graphene electrodes where the in-plane electric field $F \neq 0$ (region A) and in the InSe-capped graphene layers where $F = 0$ (region B). No significant photocurrent is observed in the graphene regions that are not capped by the InSe layer. We ascribe the large photocurrent in region A to the drift of

photogenerated carriers under the action of the applied electric field in the InSe gap between the

graphene electrodes (bottom inset, Figure 5c). We assign the smaller, but significant photocurrent

in the InSe-capped graphene layers (region B in Figure 5c) to thermal diffusion: the

photogenerated carriers diffuse in InSe and are extracted at the graphene electrodes by charge

transfer. These data demonstrate that a large photoresponse can be achieved in regions B with

distinct light-absorbing (InSe) and conducting (graphene) layers, and regions A where the InSe

layer acts simultaneously as a light-absorbing and conducting medium. The charge-transfer

mechanism for photodetection in regions B is somewhat different from that previously reported

for InSe-graphene planar and vertical photodetector structures [27] and analogous to that

demonstrated in pentacene-graphene heterostructures [28]. The light-induced transfer of charge

between InSe and graphene offers an effective method to increase or decrease the carrier density

in graphene, causing a change in its resistance and quantum Hall effect that are gate-controllable

and only weakly dependent on temperature.

From the measured values of ΔI for different incident powers, P, with an unfocused laser

beam (*i.e.* illuminating the whole area of the device), we estimate a photoresponsivity $R = \Delta I/P$ of

up to $R \sim 10^6$ A/W at the lowest incident power $P \sim 10^{-5}$ W/m^2 ($\lambda = 633$ nm) with $V_{sd} = 0.1$ V.

The photocurrent map in Figure 5c shows that both regions A and B contribute to the

photoresponse of the device. Also, the photoresponse is relatively fast with rise and decay times

of the photocurrent of less than 1 ms in both regions A and B (Figure 5d). By comparing the

photocurrent signals in areas with and without the hBN layer, we find that the encapsulation of

InSe by hBN induces a systematic increase of the signal (~ by a factor of ~ 3). We attribute this

behavior, which is not observed when the hBN layer lies below the InSe layer, to an increased

absorption of light by the InSe layer due to the reduced reflection of the laser light at the interface

between air and hBN (refractive index n_{hBN}=1.8)[29], compared to air (n_{air} = 1) and InSe (n_{InSe} = 2.7)[30]. The encapsulation of InSe by hBN also leads to an increased photoluminescence and Raman signals of InSe. In summary, these photocurrent mapping experiments demonstrate that light-induced charge-transfer at the InSe/graphene interface acts to photosensitize the graphene layer, thus enhancing its photoresponse. The response time of the photocurrent is relatively slow and is partly limited by charge traps and the *RC* time of our device structures. All measurements presented in this work are obtained under quasistatic conditions so are not influenced by dynamic polarization effects. To probe the role of dipole-dipole interactions on the photoexcited charge transfer, ultra-fast pump-probe optical spectroscopy studies and optimized device geometries are required.

3. Conclusions

In conclusion, we have demonstrated novel hybrid InSe/graphene phototransistor devices. By mounting the InSe/graphene heterostructure on an oxidized silicon substrate, we have produced devices in which the electronic properties of the graphene layer can be controlled by a combination of field effect gating and the transfer of photo-excited carriers across the InSe-graphene interface. In this way, the Fermi energy of the graphene layer can be fine-tuned across the Dirac point, thus achieving either *n*- or *p*-type conduction. The light-induced charge transfer also induces a reversal of the sign of the Hall voltage and of the $h/2e^2$ quantum Hall plateau, which extends over a wide range of applied magnetic fields and temperatures. We have measured the carrier density in the InSe and graphene layers under optical excitation. Our results demonstrate the important role of the donors in the InSe layer in determining the optical and quantum Hall characteristics of this type of device. Our hybrid phototransistor combine the high photosensitivity of InSe with the unique electrical properties of graphene. These devices are

made by a relatively simple fabrication process and offer a flexible route to integration with existing Si-manufacturing technologies. Prospects for further research include the investigation of the charge transfer in new multilayered vdW heterostructures, for example in InSe/hBN/graphene for controlled charge transfer between graphene and InSe through an intermediate tunnel hBN barrier. In particular, the broad-band absorption of InSe including a range of intraband and interband optical transitions in the visible, near-infrared and infrared range[7,9] provide an opportunity to tune the photoresponsivity of graphene and unlock its potential for optoelectronic applications, beyond the capability of traditional semiconductor devices and other 2D photodetectors in the current literature.[1, 31-33]

4. Experimental methods

The single layer graphene was grown by chemical vapor deposition (CVD) on a copper foil substrate and was transferred to a SiO_2/p-Si substrate (SiO_2 layer thickness $t = 285$ nm). The graphene was shaped into a multi-terminal Hall bar using electron-beam lithography and oxygen/argon reactive ion etching. Au/Ti electrodes (100/10 nm) were then evaporated on the graphene layer. High quality InSe flakes were exfoliated from a Bridgman-grown InSe crystal onto a polydimethylsiloxane membrane. A selected InSe flake was dry transferred to the graphene Hall bar, capping a section of the graphene channel, but not contacting the Au/Ti electrodes. Exfoliated InSe flakes capped with hBN were also integrated into two-terminal planar device structures incorporating graphene electrodes.

We performed the magneto-transport measurements with the device mounted inside a superconducting magneto-cryostat at magnetic fields B up to 14T or using a resistive magnet with B up to 25 T (Supplementary Information S2) and over a range of gate voltages, V_g, applied between the graphene and the Si-substrate. For the magneto-transport experiments under optical

illumination, we used an unfocused He-Ne laser beam (wavelength $\lambda = 632.8$ nm, power, P, up to 13 mW/mm^2, and spot diameter $d \sim 1$ mm). For the photoconductivity mapping experiments, we used a focused laser beam (wavelength $\lambda = 405$ nm and spot diameter $d \sim 1$ μm).

ASSOCIATED CONTENT

Additional data on the magnetoresistance, the quantum Hall plateau and the parallel conduction along the InSe layer are in the Supplementary Information.

REFERENCES

[1] A. C. Ferrari, F. Bonaccorso, V. I. Fal′ko, K. S. Novoselov, S. Roche, P. Bøggild, S. Borini, F. H. L. Koppens, V. Palermo, N. Pugno, J. A. Garrido, R. Sordan, A. Bianco, L. Ballerini, M. Prato, E. Lidorikis, J. Kivioja, C. Marinelli, T. Ryhänen, A. Morpurgo, J. N. Coleman, V. Nicolosi, L. Colombo, A. Fert, M. Garcia-Hernandez, A. Bachtold, G. F. Schneider, F. Guinea, C. Dekker, M. Barbone, Z. Sun, C. Galiotis, A. N. Grigorenko, G. Konstantatos, A. Kis, M. Katsnelson, L. Vandersypen, A. Loiseau, V. Morandi, D. Neumaier, E. Treossi, V. Pellegrini, M. Polini, A. Tredicucci, G. M. Williams, B. H. Hong, J. -H. Ahn, J. M. Kim, H. Zirath, B. J. van Wees, H. van der Zant, L. Occhipinti, A. D. Matteo, I. A. Kinloch, T. Seyller, E. Quesnel, X. Feng, K. Teo, N. Rupesinghe, P. Hakonen, S. R. T. Neil, Q. Tannock, T. Löfwander, J. Kinaret, *Nanoscale* **2015**, *7*, 4598.

[2] A. K. Geim, I. V. Grigorieva, *Nature* **2013**, *499*, 419.

[3] L. Ci, L. Song, C. Jin, D. Jariwala, D. Wu, Y. Li, A. Srivastava, Z. F. Wang, K. Storr, L. Balicas, F. Liu, P. M. Ajayan, *Nat. Mater.* **2010**, *9*, 430.

[4] J. Yang, S. Tran, J. Wu, S. Che, P. Stepanov, T. Taniguchi, K. Watanabe, H. Baek, D. Smirnov, R. Chen, C. N. Lau, *Nano Lett.* **2018**, *18*, 229.

[5] Q. H. Wang, K. Kalantar-Zadeh, A. Kis, J. N. Coleman, M. S. Strano, *Nat. Nanotechnol.* **2012**, *7*, 699.

[6] K. Wang, K. De Greve, L. A. Jauregui, A. Sushko, A. High, Y. Zhou, G. Scuri, T. Taniguchi, K. Watanabe, M. D. Lukin, H. Park, P. Kim, *Nat. Nanotechnol.* **2018**, *13*, 128.

[7] G. W. Mudd, M. R. Molas, X. Chen, V. Zólyomi, K. Nogajewski, Z. R. Kudrynskyi, Z. D. Kovalyuk, G. Yusa, O. Makarovsky, L. Eaves, M. Potemski, V. I. Fal′ko, A. Patanè, *Sci. Rep.* **2016**, *6*, 39619.

[8] M. Brotons-Gisbert, D. Andres-Penares, J. Suh, F. Hidalgo, R. Abargues, P. J. Rodríguez-Cantó, A. Segura, A. Cros, G. Tobias, E. Canadell, P. Ordejón, J. Wu, J. P. Martínez-Pastor, J. F. Sánchez-Royo, *Nano Lett.* **2016**, *16*, 3221.

[9] D. A. Bandurin, A. V. Tyurnina, G. L. Yu, A. Mishchenko, V. Zólyomi, S. V. Morozov, R. K. Kumar, R. V. Gorbachev, Z. R. Kudrynskyi, S. Pezzini, Z. D. Kovalyuk, U. Zeitler, K. S. Novoselov, A. Patanè, L. Eaves, I. V. Grigorieva, V. I. Fal′ko, A. K. Geim, Y. Cao, *Nat. Nanotechnol.* **2017**, *12*, 223.

[10] W. Feng, W. Zheng, W. Cao, P. A. Hu, *Adv. Mater.* **2014**, *26*, 6587.

[11] M. Hamer, E. Tóvári, M. Zhu, M. D. Thompson, A. Mayorov, J. Prance, Y. Lee, R. P. Haley, Z. R. Kudrynskyi, A. Patanè, D. Terry, Z. D. Kovalyuk, K. Ensslin, A. V. Kretinin, A. Geim, R. Gorbachev, *Nano Lett.* **2018**, *18*, 3950.

[12] N. Balakrishnan, Z. R. Kudrynskyi, E. F. Smith, M. W. Fay, O. Makarovsky, Z. D. Kovalyuk, L. Eaves, P. H. Beton, A. Patanè, *2D Mater.* **2017**, *4*, 025043.

[13] Z. R. Kudrynskyi, M. A. Bhuiyan, O. Makarovsky, J. D. G. Greener, E. E. Vdovin, Z. D. Kovalyuk, Y. Cao, A. Mishchenko, K. S. Novoselov, P. H. Beton, L. Eaves, A. Patanè, *Phys. Rev. Lett.* **2017**, *119*, 157701.

[14] Z. Chen, J. Biscaras, A. Shukla, *Nanoscale* **2015**, *7*, 5981.

[15] A. A. Kistanov, Y. Cai, K. Zhou, S. V. Dmitriev, Y. -W. Zhang, *Phys. Chem. Chem. Phys.* **2018**, *20*, 12939.

[16] S. Zhou, C. -C. Liu, J. Zhao, Y. Yao, *npj Quantum Materials* **2018**, doi:10.1038/s41535-018-0089-0.

[17] G. W. Mudd, A. Patanè, Z. R. Kudrynskyi, M. W. Fay, O. Makarovsky, L. Eaves, Z. D. Kovalyuk, V. Zólyomi, V. I. Fal′ko, *Appl. Phys. Lett.* **2014**, *105*, 221909.

[18] Y. Lee, R. Pisoni, H. Overweg, M. Eich, P. Rickhaus, A. Patanè, Z. R. Kudrynskyi, Z. D. Kovalyuk, R. Gorbachev, K. Watanabe, T. Taniguchi, T. Ihn, K. Ensslin, *2D Mater.* **2018**, *5*, 035040.

[19] Y. Sun, S. Luo, X. -G. Zhao, K. Biswas, S. -L. Li, L. Zhang, *Nanoscale* **2018**, *10*, 7991.

[20] K. S. Novoselov, A. K. Geim, S. V. Morozov, D. Jiang, M. I. Katsnelson, I. V. Grigorieva, S. V. Dubonos, A. A. Firsov, *Nature* **2005**, *438*, 197.

[21] Y. Zhang, Y. -W. Tan, H. L. Stormer, P. Kim, *Nature* **2005**, *438*, 201.

[22] A. Tzalenchuk, S. Lara-Avila, A. Kalaboukhov, S. Paolillo, M. Syväjärvi, R. Yakimova, O. Kazakova, T. J. B. M. Janssen, V. I. Fal′ko, S. Kubatkin, *Nat. Nanotechnol.* **2010**, *5*, 186.

[23] S. Kopylov, A. Tzalenchuk, S. Kubatkin, V. I. Fal′ko, *Appl. Phys. Lett.* **2010**, *97*, 112109.

[24] T. J. B. M. Janssen, A. Tzalenchuk, S. Lara-Avila, S. Kubatkin, V. I. Fal′ko, *Rep. Prog. Phys.* **2013**, *76*, 104501.

[25] R. Ribeiro-Palau, F. Lafont, J. Brun-Picard, D. Kazazis, A. Michon, F. Cheynis, O. Couturaud, C. Consejo, B. Jouault, W. Poirier, F. Schopfer, *Nat. Nanotechnol.* **2015**, *10*, 965.

[26] J. A. Alexander-Webber, J. Huang, D. K. Maude, T. J. B. M. Janssen, A. Tzalenchuk, V. Antonov, T. Yager, S. Lara-Avila, S. Kubatkin, R. Yakimova, R. J. Nicholas, *Sci. Rep.* **2016**, *6*, 30296.

[27] G.W. Mudd, S.A. Svatek , L. Hague, O. Makarovsky, Z.R. Kudrynskyi, C. J. Mellor, P.H. Beton , L. Eaves , K. S. Novoselov, Z.D. Kovalyuk, E.E. Vdovin, A.J. Marsden , N.R. Wilson, A. Patanè, *Adv. Mater.* **2015**, *27*, 3760.

[28] X. Chen, X. Liu, B. Wu, H. Nan, H. Guo, Z. Ni, F. Wang, X. Wang, Y. Shi, X. Wang, *Nano Lett.* **2017**, *17,* 6391.

[29] S. L. Rumyantsev, M. E. Levinshtein, A. D. Jackson, S. N. Mohammad, G. L. Harris, M. G. Spencer, M. S. Shur, in *Properties of Advanced Semiconductor Materials GaN, AlN, InN, BN, SiC, SiGe* (Eds: M. E. Levinshtein, S. L. Rumyantsev, M. S. Shur), John Wiley & Sons, Inc., New York **2001**, pp. 67-92.

[30] F. J. Manjón, Y. van der Vijver, A. Segura, V. Muñoz, *Semicond. Sci. Technol*. **2000**, *15*, 806.

[31] F. H. L. Koppens, T. Mueller, Ph. Avouris, A. C. Ferrari, M. S. Vitiello, M. Polini, *Nat. Nanotechnol.* **2014**, *9*, 780.

[32] F. Yan, L. Zhao, A. Patanè, P. A. Hu, X. Wei, W. Luo, D. Zhang, Q. Lv, Q. Feng, C. Shen, K. Chang, L. Eaves, K. Wang, *Nanotechnology* **2017**, *28*, 27LT01.

[33] S. Goossens, G. Navickaite, C. Monasterio, S. Gupta, J. J. Piqueras, R. Pérez, G. Burwell, I. Nikitskiy, T. Lasanta, T. Galán, E. Puma, A. Centeno, A. Pesquera, A. Zurutuza, G. Konstantatos, F. Koppens, *Nat. Photonics* **2017**, *11*, 366.
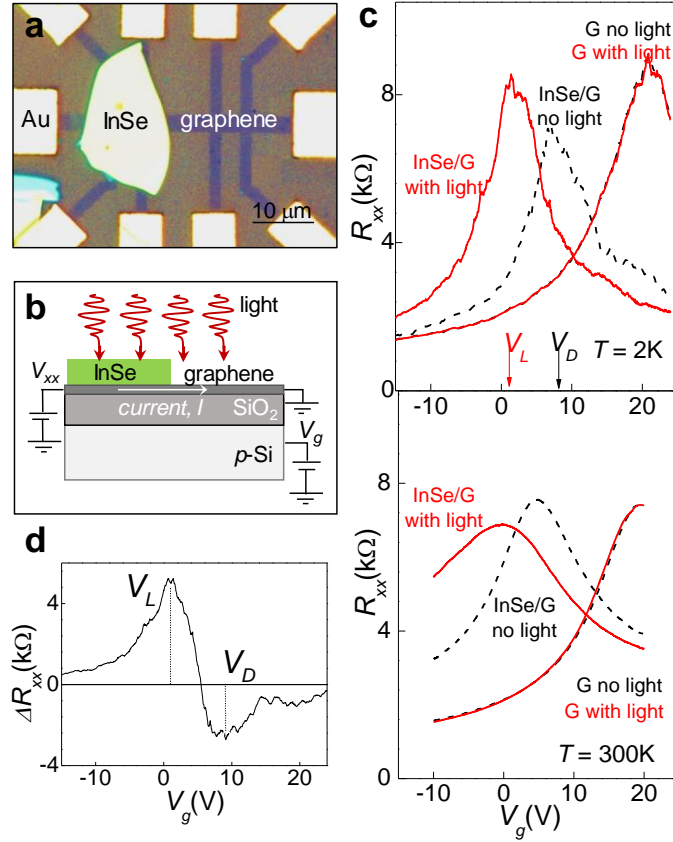
Figure 1. (a) Optical image and (b) sketch of a Hall bar containing uncapped and InSe-capped graphene. The thickness of the InSe layer is 50 nm, as measured by atomic force microscopy. Devices with different layer thickness down to ~ 10 nm show a similar behaviour. (c) Resistance R_{xx} versus gate bias V_g ($B = 0$T and $I = 0.5$ μA) without (black curves) and with illumination (red curves; $\lambda = 633$ nm and $P = 9$ mW/mm^2) for uncapped graphene (G) and InSe-capped graphene (InSe/G). Top: $T = 2$ K; Bottom: $T = 300$K. V_L and V_D denote the peak position of the $R_{xx}(V_g)$ curves under illumination and in darkness, respectively. (d) Dependence on the gate voltage V_g of the change in the resistance, ΔR_{xx}, of the InSe-capped section of the graphene Hall bar after illumination.
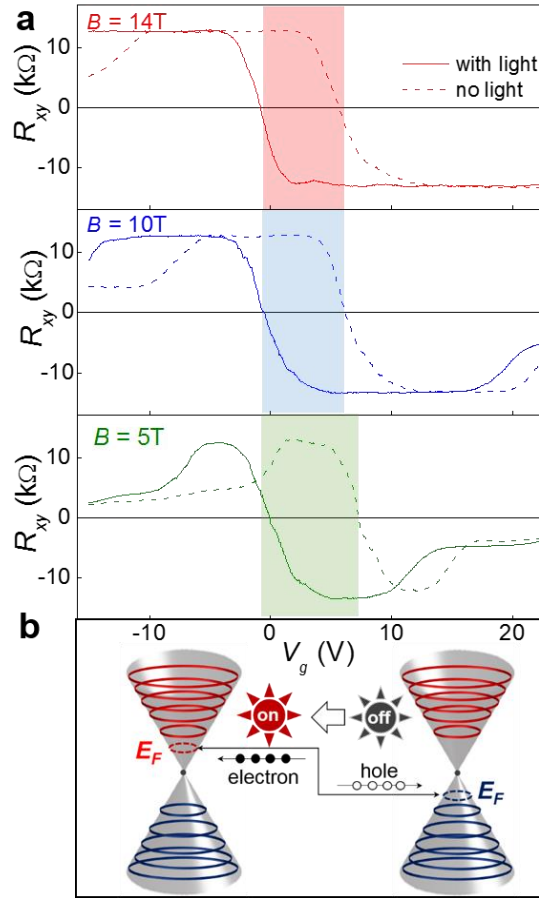
Figure 2. (a) Hall resistance, R_{xy}, of InSe-capped graphene versus gate voltage, V_g, in darkness (dashed line) and under illumination (continuous line) at $T = 2$ K and $B = 5$, 10 and 14T ($I = 0.5$ μA, $\lambda = 633$nm and $P = 9$mW/mm^2). The shaded areas identify a range of gate voltages for which light reverses the sign of R_{xy}. (b) Landau level quantization in graphene and sketch of the movement of the Fermi level from the lower to the upper part of the Dirac cone under illumination, leading to the sign reversal of R_{xy} shown in part (a).
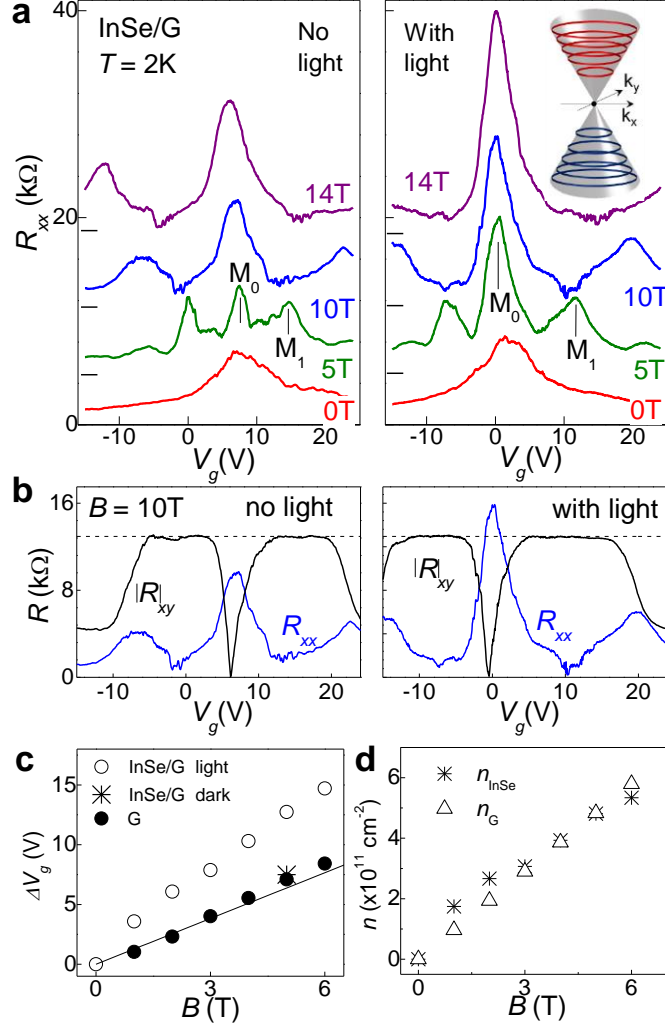
Figure 3. (a) Resistance, R_{xx}, of InSe-capped graphene versus gate voltage, V_g, at various applied magnetic fields B in darkness (left) and under illumination (right) ($T = 2$ K, $\lambda = 633$nm, $P = 9$mW/mm^2). For clarity, curves at different B are displaced along the vertical axis. M_0 and M_1 label two maxima in $R_{xx}(V_g)$ corresponding to the alignment of the Fermi level with the $i = 0$ and $i =+1$ Landau levels (LLs). Inset: LL quantization in graphene. (b) R_{xx} and modulus of the Hall resistance, $|R_{xy}|$ versus V_g in darkness (left) and under illumination (right) at $B = 10$ T. Dashed lines show $R_{xy} = h/2\,e^2$. (c) B-dependence of the separation, ΔV_g, between peaks in $R_{xx}(V_g)$, M_0 and M_1, for graphene (G) and InSe-capped graphene (InSe/G) in darkness and under illumination ($T = 2$K). The line is the calculated dependence for graphene according to the model described in the text. (d) Density of carriers in graphene (n_G) and donor states in InSe (n_{InSe}) versus B for InSe-capped graphene.
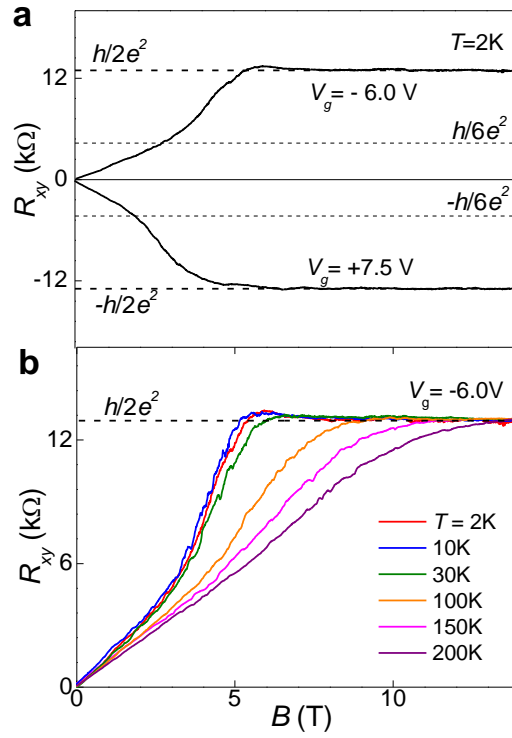
Figure 4. (a) Hall resistance, R_{xy}, of InSe-capped graphene versus magnetic field B at $T = 2$ K and different gate voltages V_g under illumination ($I = 0.5$ µA, $\lambda = 633$nm and $P = 9$mW/mm^2). (b) Hall resistance R_{xy} of InSe-capped graphene versus B under illumination at different temperatures, T, and $V_g = -6.0$V ($I = 0.5$ µA, $\lambda = 633$nm and $P = 9$mW/mm^2).
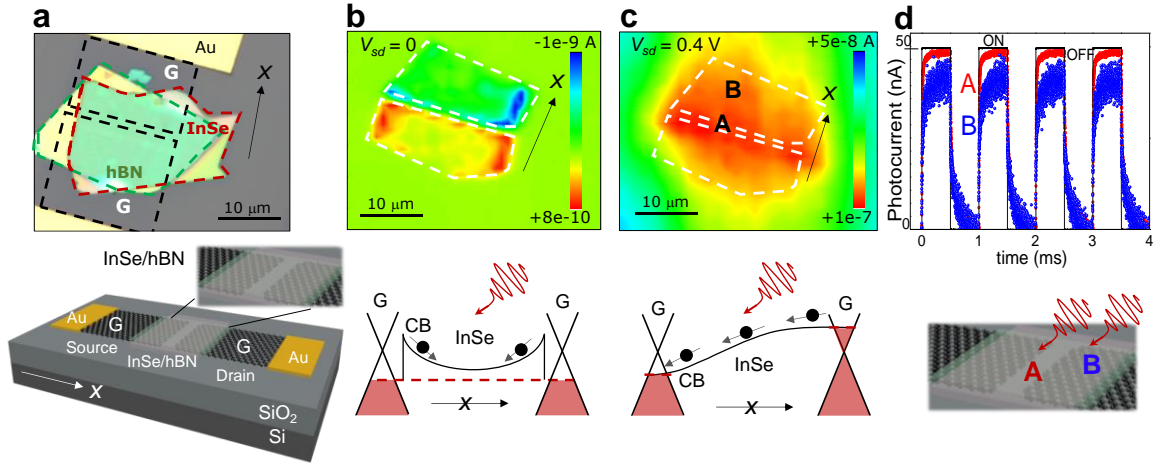
Figure 5. (a) Optical image and diagram of a graphene-InSe/hBN-graphene planar device with regions of overlaps between the InSe (red line), hBN (green lines) and graphene (black lines) layers. (b-c) Photocurrent maps acquired without (b) and with (c) an applied source-drain voltage, V_{sd}, between two graphene electrodes at $T = 300$ K ($\lambda = 405$ nm and $P = 50$ μW). In part (b), the photocurrent ΔI is generated in the region of overlap between the InSe and graphene electrodes (indicated by dashed white lines) and is enhanced at the graphene edges ($V_{sd} = 0.4$ V). In part (c), the photocurrent ΔI is generated in the gap between the graphene electrodes (region A) and in the InSe-capped graphene layers (region B). Insets: Photocurrent generation by the built-in electric field at the graphene/InSe interface (b) and by drift (or thermal diffusion) of photogenerated carriers (c). (d) Temporal dependence of the photocurrent in regions A and B.

Supplementary Information

Photo-quantum Hall effect and light-induced charge transfer

at the interface of graphene/InSe heterostructures

Mahabub A. Bhuiyan[1], Zakhar R. Kudrynskyi[1], Debarati Mazumder[1], Jake D.G. Greener[1],

Oleg Makarovsky[1], Christopher J. Mellor[1], Evgeny E. Vdovin[1, 2], Benjamin A. Piot[3], Inna I.

Lobanova[3], Zakhar D. Kovalyuk[4], Marina Nazarova[5, 6], Artem Mishchenko[5], Kostya S.

Novoselov[5], Yang Cao[6-7], Laurence Eaves[1], Go Yusa[8], Amalia Patanè[1*

[1] School of Physics and Astronomy, The University of Nottingham, Nottingham NG7 2RD, UK

[2] Institute of Microelectronics Technology and High Purity Materials, RAS,

Chernogolovka 142432, Russia

[3] Laboratoire National des Champs Magnétiques Intenses, CNRS-UGA-UPS-INSA-EMFL,

25 rue des Martyrs, 38042 Grenoble, France

[4] Institute for Problems of Materials Science, The National Academy of Sciences of Ukraine,

Chernivtsi Branch, Chernivtsi 58001, Ukraine

[5] School of Physics and Astronomy, University of Manchester, Oxford Road,

Manchester M13 9PL, UK

[6] National Graphene Institute, University of Manchester, Oxford Road, Manchester M13 9PL, UK

[7] State Key Laboratory of Physical Chemistry of Solid Surface, College of Chemistry and

Chemical Engineering, Collaborative Innovation Center of Chemistry for Energy Materials,

Xiamen University, Xiamen, 361005, China

[8] Department of Physics, Tohoku University, Sendai 980-8578, Japan

*Corresponding author: amalia.patane@nottingham.ac.uk

S1. Effect of light on R_{xx} for InSe-capped graphene

The V_g-dependence of the room temperature ($T = 300$K) resistance, R_{xx}, of the InSe-capped graphene was measured in darkness and under illumination, Figure S1a. In darkness R_{xx} reaches a maximum at a positive gate voltage, corresponding to a p-type character at $V_g = 0$. We estimate the hole density from the capacitance equation $p = -CV_g/q$. Here $q = -e$ is the electron charge, $C = \varepsilon\varepsilon_0/t = 121$ μF/m^2 is the "classical" capacitance per unit area of the graphene/SiO$_2$/Si heterostructure, $t = 285$ nm is the SiO$_2$ layer thickness, $\varepsilon = 3.9$ is the relative dielectric constant of SiO$_2$, ε_0 is the permittivity of free space, and V_g is the voltage position of the peak in $R_{xx}(V_g)$.

The maximum of $R_{xx}(V_g)$ shifts steadily towards lower bias with increasing light intensity. The shift to lower bias, ΔV_g, is proportional to the light intensity at low levels, but tends to saturate at $P \approx 10$ mW/mm^2. Thus R_{xx} is either increased or decreased by light depending on the applied gate voltage and/or light intensity. This is illustrated in Figure S1b showing the V_g-dependence of the light-induced change of R_{xx}, ΔR_{xx}, at $T = 300$K. We use the measured value of ΔV_g and the capacitance equation

$$\Delta n = C\Delta V_g/q \tag{S1}$$

to estimate the light-induced increase in electron density Δn, Figure S1c. This increase is attributed to a photogating effect, as described in the main text and sketched in Figure S1d.
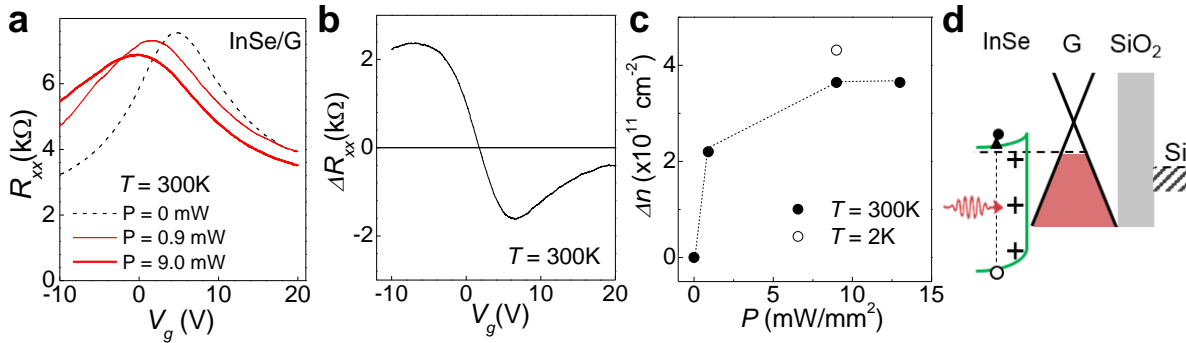

Figure S1. (a) Resistance R_{xx} of InSe-capped graphene versus V_g ($I=0.5$μA) under illumination ($P = 0$, 0.9, 9.0 mW/mm^2; $\lambda = 633$ nm) at $B = 0$T and $T = 300$ K. (b) Dependence of ΔR_{xx}, the change in the resistance R_{xx} after light illumination, on V_g ($P = 9.0$ mW/mm^2 and $T = 300$K). (c) Change in the electron density after light illumination as derived from the voltage shift of the R_{xx} (V_g) curve and the capacitance equation described in the text. (d) Band diagram for the InSe/graphene/SiO$_2$/Si heterostructure under illumination.

S2. Quantum Hall plateau in InSe-capped graphene

The quantum Hall (QH) plateau at a filling factor $v = 2$ in the magnetic field-dependent Hall resistance, R_{xy}, of InSe-capped CVD graphene extends up to the highest available magnetic field, *i.e.* $B = 25$ T, at $T = 2$ K. A similar extended QH plateau at a filling factor $v = 2$ is also observed in InSe-capped exfoliated graphene on an hBN/SiO$_2$/Si substrate, see Figure S3.
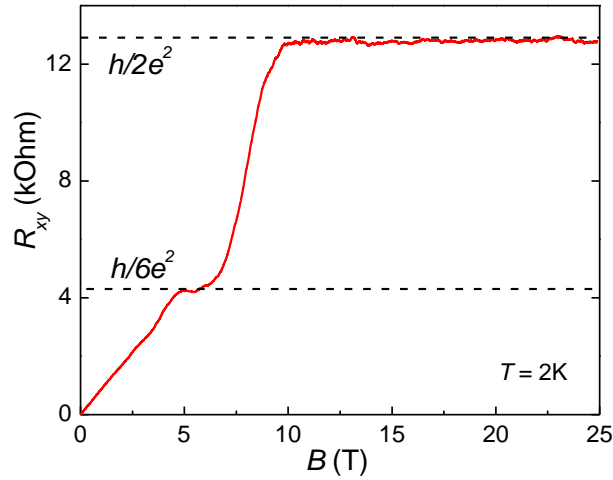

Figure S2. Hall resistance R_{xy} of InSe-capped CVD graphene versus magnetic field B measured in the darkness at $V_g = +22$V ($I = 0.5$ μA) and $T = 2$ K.
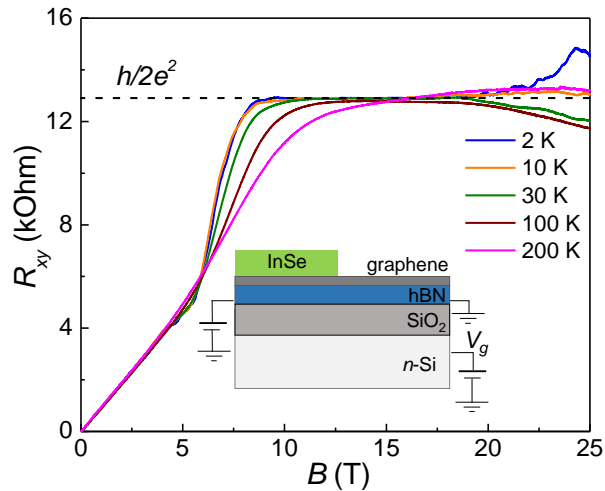

Figure S3. Hall resistance R_{xy} of InSe-capped exfoliated graphene versus B in the dark at different temperatures, T, and $V_g = + 8.0$V ($I = 0.5$ μA). Inset: schematic representation of the InSe/exfoliated graphene on an hBN/SiO$_2$/Si substrate.

S3. Parallel conduction along the InSe layer in InSe-capped graphene Hall bars

To examine the parallel conduction along the InSe layer, we model the Hall resistance R_{xy} in the high field and quantum limit as[1]:

$$R_{xy} = \frac{B}{en_p + 2Be^2/h},\tag{S2}$$

where n_p is the density of free electrons in the parallel InSe conducting layer. As shown in Figure 4 of the main text, at $T = 2K$, the quantized value of $R_{xy} = h/2e^2$ indicates that parallel conduction can be neglected at this temperature. However, with increasing T, R_{xy} decreases below its quantized value, thus indicating a thermally activated increase of n_p and current leaking across the InSe layer. Using the measured values of R_{xy} at various T and equation S2, we find that n_p increases with increasing T. In particular, at $B = 12T$ it increases from zero at 2K to $\sim 10^{10}$ cm^{-2} at $T \sim 200K$ (Figure S4).
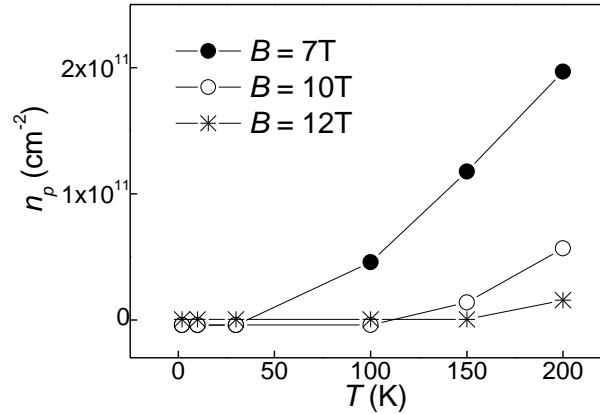

Figure S4. Carrier density in the InSe layer versus T, as derived from a fit to the measured values of R_{xy} to equation S2 at different applied magnetic fields B.

S4. Quantum and classical capacitance

The total capacitance, C, of the InSe/graphene/SiO$_2$/Si heterostructure, is a series combination of the classical capacitance, C_c, and the quantum capacitance, C_q, of graphene: $C^{-1} = C_c^{-1} + C_q^{-1}$. The classical capacitance is $C_c = \varepsilon\varepsilon_0/t = 121$ μF/m^2, where $t = 285$ nm is the SiO$_2$ layer thickness and $\varepsilon = 3.9$ is the relative dielectric constant of SiO$_2$. The quantum

capacitance accounts for the non-classical dependence of the graphene's carrier density, n_G, on the applied gate voltage V_g when the Fermi energy, E_F, is close to the low density of states at the Dirac point: $C_q = e^2(dn_G/dE_F) = 2e^2 \frac{E_F}{\pi\hbar^2 v_F^2}$ [2]. As shown in Figure S5, when the Fermi level is far from the Dirac point ($E_F = 0$), the contribution of the quantum capacitance becomes negligible compared to that of the classical capacitance. The range of values of E_F and V_g that we consider to model the voltage separation of the maxima M_0 and M_1 in $R_{xx}(V_g)$ correspond to $\Delta V_g > 1$V ($\Delta E_F > 30$ meV). The corresponding values of C_q are too high to observe a measurable deviation of C from C_c. In general, an important effect of the quantum capacitance is expected in devices with a large classical capacitance C_c (10^4 µF/m^2) [2].
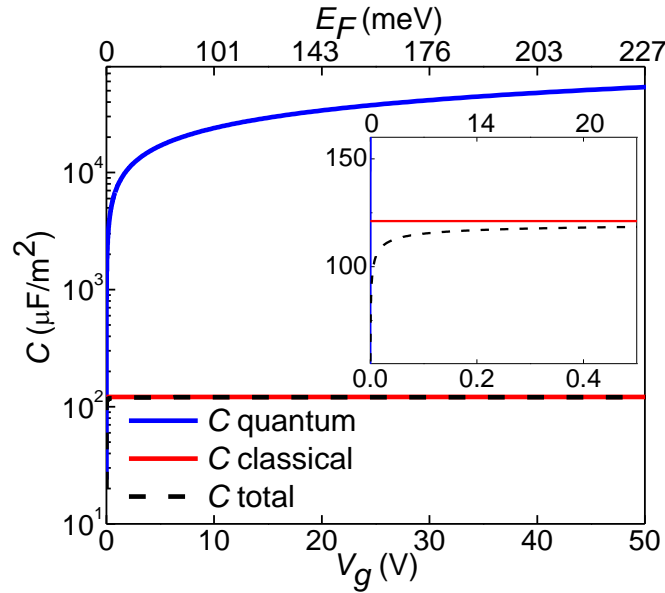

Figure S5 Dependence of the quantum, classical and total capacitance on the gate voltage (bottom x-axis) and Fermi energy (top x-axis). The inset shows the dependence over a narrow range of Fermi energies in the close vicinity of the Dirac point.

References

[1] M. A. Reed, W. P. Kirk, P. S. Kobiela, *IEEE J. Quantum Electron.* **1986**, *22*, 1753.

[2] L. A. Ponomarenko et al., *Phys Rev Lett* **2010,** *105*, 136801.